ELSEVIER

Volume 182, Number 8, August 2009

JOURNAL OF SOLID STATE CHEMISTRY

www.elsevier.com/locate/jssc

# CONTENTS

Abstracted/indexed in BioEngineering Abstracts, Chemical Abstracts, Coal Abstracts, Current Contents/Physics, Chemical, & Earth Sciences, Engineering Index, Research Alert, SCISEARCH, Science Abstracts, and Science Citation Index. Also covered in the abstract and citation database SCOPUS®. Full text available on ScienceDirect®.

## Regular Articles

**Phase diagram of the La–Si binary system under high pressure and the structures of superconducting $LaSi_5$ and $LaSi_{10}$**
Shoji Yamanaka, Satoshi Izumi, Shoichi Maekawa and Keita Umemoto
***Page 1991***

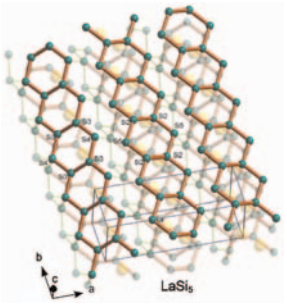


In the study of the phase diagram of the La–Si binary system under high pressure and high temperature conditions, new Si-rich superconducting $LaSi_5$ ($T_c = 11.5$ K) and $LaSi_{10}$ ($T_c = 6.7$ K) have been found. $LaSi_5$ contain unique one-dimensional sila-polyacene ribbons, and $LaSi_{10}$ has a hexagonal columnar structure formed by face shared La@$Si_{18}$ polyhedra.

**Synthesis, crystal structure and characterization of iron pyroborate ($Fe_2B_2O_5$) single crystals**
Tetsuya Kawano, Haruhiko Morito, Takahiro Yamada, Takeyoshi Onuma, Shigefusa F. Chichibu and Hisanori Yamane
***Page 2004***

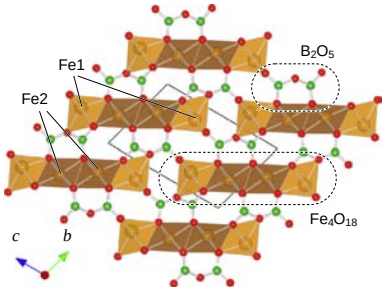


View of the crystal structure of $Fe_2B_2O_5$ using $FeO_6$ octahedra. $Fe_2B_2O_5$ has a quasi-one-dimensional structure, consisting of an [$Fe_4O_{18}$] unit parallel to the *a*-axis.

## Regular Articles—Continued

**Grafting of organosilane derived from 3-glycidoxypropyltrimethoxysilane and thiourea onto magnesium phyllosilicate by sol–gel process and investigation of metal adsorption properties**
R.K. Dey, Andrea S. Oliveira, Tanushree Patnaik, V.K. Singh, D. Tiwary and Claudio Airoldi
***Page 2010***

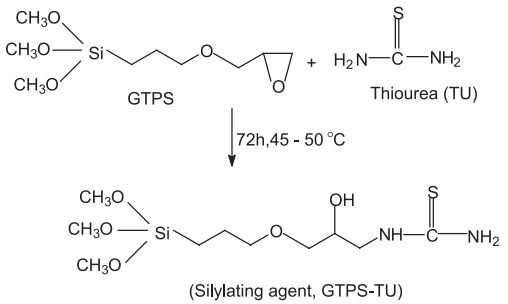


We report the synthesis and adsorption properties of a layered inorganic–organic magnesium silicate (Mg-GTPS-TU) derived from a new silylaing agent from 3-glycidoxypropyltrimethoxysilane (GTPS) and thiourea (TU) as the silicon source.

**Magnetic properties of the spinel-type $Cu(Cr_{1-x}Hf_x)_2S_4$**
F. Kariya, K. Ebina, K. Hasegawa, K. Koshimizu, B. Wuritunasitu, K. Hondou, S. Ebisu and S. Nagata
***Page 2018***

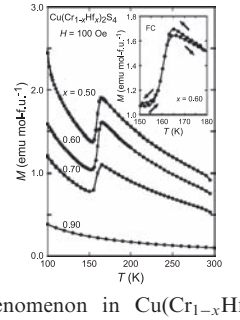


Spin crossover phenomenon in $Cu(Cr_{1-x}Hf_x)_2S_4$. A step-like anomaly is found around 160 K for $x = 0.50$, 0.60, and 0.70 in the magnetization as a function of temperature. The inset shows the enlargement data for $x = 0.60$. This crossover indicates that the spin state changes from high temperature $S = 2$ to low temperature $S = \frac{3}{2}$ states.

*Continued*

**High-pressure synthesis and structures of lanthanide germanides of $LnGe_5$ ($Ln$ = Ce, Pr, Nd, and Sm) isotypic with $LaGe_5$**

Hiroshi Fukuoka, Kazuya Baba, Mayumi Yoshikawa, Fumiko Ohtsu and Shoji Yamanaka

***Page 2024***

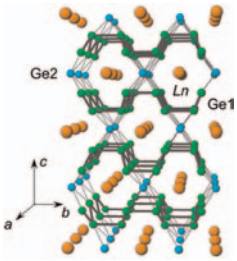


A series of lanthanide penta-germanides $LnGe_5$ ($Ln$ = Ce, Pr, Nd and Sm) has been prepared by high-pressure (5–13 GPa) and high-temperature (500–1200 °C) reaction.

---

**Phase transition behavior for $ZrW_{2-x}Mo_xO_8$ compositions at elevated temperatures**

Yongfang Shi, Xi Chen, Jingsa Han, Hui Ma, Xiaoxia Li, Xiaojing Yang and Xinhua Zhao

***Page 2030***

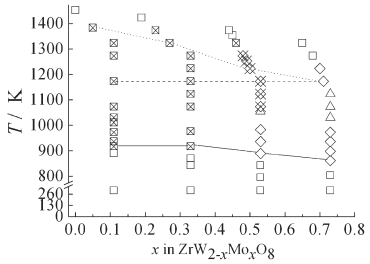


The phase behavior–temperature relationship of $ZrW_{2-x}Mo_xO_8$ system. The phase denoted with symbol: (□): cubic; (△): trigonal; (×): oxides; (◇): cubic and trigonal; (⊠): cubic and oxides; (⊗): cubic, trigonal and oxides. The temperature threshold of phase transition: (—); metastable cubic transition; (- - - - -): $MoO_3$ sublimation; (·····): reaction to form W-rich $ZrW_{2-x}Mo_xO_8$.

---

**Phase diagram features and solidification behaviour of $CoCu_2O_3$ at elevated oxygen pressure**

N. Wizent, L. Schramm, G. Behr, W. Löser, W. Gruner, A. Voß, B. Büchner and L. Schultz

***Page 2036***

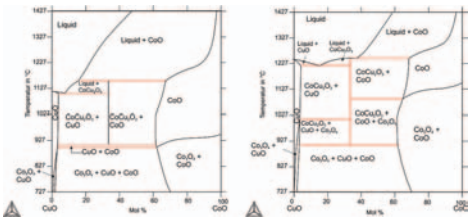

A unique behaviour of the phase $CoCu_2O_3$ was found both from CALPHAD calculations and directional solidification experiments. For elevated oxygen partial pressure the solidification mode changed from double-peritectic (1 bar $O_2$; left figure) to a congruent melting behaviour with respect to the metals (Cu, Co) and to the oxygen content (80 bar $O_2$; right figure).

**Polymerization of aniline in the interlayer space of molybdenum trioxide and its electrochemical properties**

Yanping Li, Yixian Xiang, Xiaowen Dong, Jiaqiang Xu, Fei Ruan and Qingyi Pan

***Page 2041***

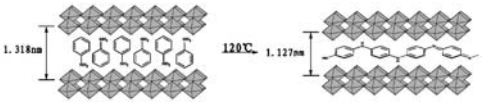


Aniline (ANI) monomer was intercalated into the interlayer space of molybdenum trioxide ($MoO_3$) and heat-treated at 120 °C for 3 d in air, and then polymerized to form layered structure of molybdenum trioxide/polyaniline ($MoO_3$/PANI) composite. Its interlayer spacing of $MoO_3$/PANI composite is 1.127 nm.

---

**Synthesis and structure analysis of tetragonal $Li_7La_3Zr_2O_{12}$ with the garnet-related type structure**

Junji Awaka, Norihito Kijima, Hiroshi Hayakawa and Junji Akimoto

***Page 2046***

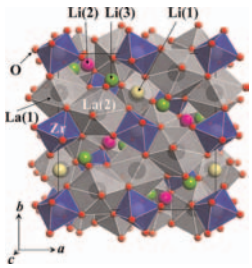


Garnet-related $Li_7La_3Zr_2O_{12}$ having tetragonal symmetry ($I4_1/acd$, no.142) has been successfully synthesized. Single crystals have been also grown by a flux method. The single-crystal X-ray diffraction analysis verifies that tetragonal $Li_7La_3Zr_2O_{12}$ has the garnet-related type structure with the lattice constants of $a$ = 13.134(4) Å and $c$ = 12.663(8) Å and the fully ordered arrangement of Li atoms.

---

**$VNb_9O_{25-\delta}$—Synthesis, electrical conducting behaviour and density functional theory (DFT) calculation**

Carina Bergner, Vladimir Vashook, Stefano Leoni and Hubert Langbein

***Page 2053***

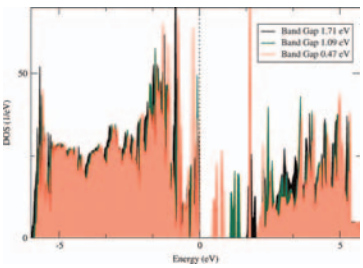


The electrical conductivity of the $n$-type semiconductor $VNb_9O_{25-\delta}$ can be interpreted as an activated hopping process with a preferred localisation of charge carriers at V(IV) centres. The electronic structure of $VNb_9O_{25-\delta}$ was calculated within the framework of the local density approximation (LDA) to DFT. The partial reduction of V(V) centres causes localised vanadium states to appear inside the band gap.

**Preparation, characterization of the Ta-doped ZnO nanoparticles and their photocatalytic activity under visible-light illumination**

Ji-Zhou Kong, Ai-Dong Li, Hai-Fa Zhai, You-Pin Gong, Hui Li and Di Wu

***Page 2061***

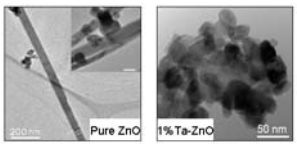


The addition of the tantalum into ZnO prepared by a modified polymerizable complex method not only restrains the growth of crystal, minish the particle size, but also changes the nanocrystal morphology.

---

**Vibrational properties of the gallium monohydrides SrGaGeH, BaGaSiH, BaGaGeH, and BaGaSnH**

Michael J. Evans, Myeong H. Lee, Gregory P. Holland, Luke L. Daemen, Otto F. Sankey and Ulrich Häussermann

***Page 2068***

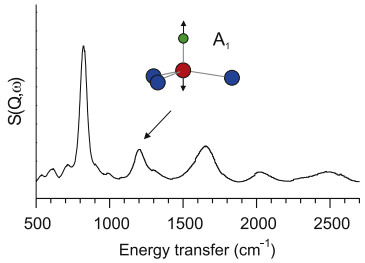


Vibrational properties of the gallium monohydrides SrGaGeH, BaGaSiH, BaGaGeH, and BaGaSnH have been investigated and revealed Ga–H stretching mode frequencies around 1200 $cm^{-1}$. This implies that the terminal Ga–H bond in solid state polyanionic gallium hydrides is very weak compared to molecular gallium hydride species.

---

**Rubidium uranyl phosphates and arsenates with polymeric tetrahedral anions: Syntheses and structures of $Rb_4[(UO_2)_6(P_2O_7)_4(H_2O)]$, $Rb_2[(UO_2)_3(P_2O_7)(P_4O_{12})]$ and $Rb[(UO_2)_2(As_3O_{10})]$**

Evgeny V. Alekseev, Sergey V. Krivovichev and Wulf Depmeier

***Page 2074***

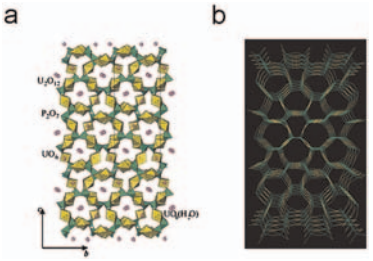


The polyhedral (a) and topological (b) representation of the $Rb_4[(UO_2)_6(P_2O_7)_4(H_2O)]$ crystal structure.

**Constructing magnetic polyaniline/metal hybrid nanostructures using polyaniline/$Fe_3O_4$ composite hollow spheres as supports**

Lirong Kong, Xiaofeng Lu, E Jin, Shan Jiang, Xiujie Bian, Wanjin Zhang and Ce Wang

***Page 2081***

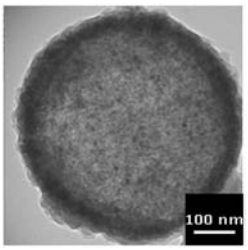


TEM image of PANI/$Fe_3O_4$ hollow spheres which can be used as supports for a variety of catalysts such as noble metal nanoparticles. Based on the unique properties of polyaniline hollow spheres and $Fe_3O_4$ NPs, we designed the synthesis of polyaniline/$Fe_3O_4$ NPs composite hollow spheres as supports for catalysts such as noble metal NPs. As a result, the obtained composites exhibit enhanced catalytic activities and can be easily separated from reaction mixture by using an NdFeB permanent magnet.

---

**Transport and mechanical property evaluation of $(AgSbTe)_{1-x}(GeTe)_x$ ($x = 0.80, 0.82, 0.85, 0.87, 0.90$)**

James R. Salvador, J. Yang, X. Shi, H. Wang and A.A. Wereszczak

***Page 2088***

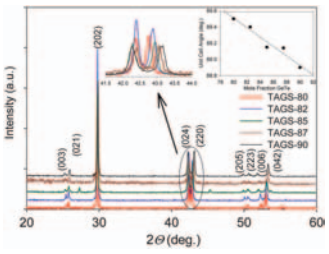


Powder X-ray diffraction of TAGS-$x$ ($x = 0.80$, 0.82, 0.85, 0.87 and 0.90) showing characteristic bifurcation indicative of rhombohedral structure.

---

**Orthorhombic–orthorhombic phase transitions in $Nd_2NiO_{4+\delta}$ ($0.067 \leq \delta \leq 0.224$)**

Kenji Ishikawa, Kenji Metoki and Hiroshi Miyamoto

***Page 2096***

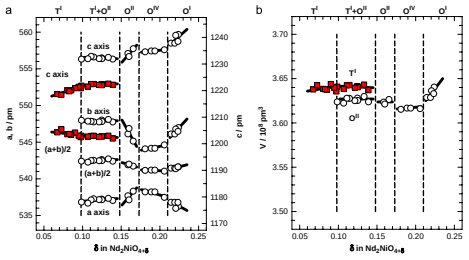


Variation of (a) the lattice constants and (b) the cell volume at room temperature of $Nd_2NiO_{4+\delta}$ with the excess oxygen concentration. $O^{I}$: orthorhombic-I; $O^{II}$: orthorhombic-II; $O^{IV}$: orthorhombic-IV; $T^{I}$: quasi-tetragonal-I.

*Continued*

**Synthesis and magnetic properties of $ALnO_2$ ($A$ = Cu or Ag; $Ln$ = rare earths) with the delafossite structure**
Naoyuki Miyasaka, Yoshihiro Doi and Yukio Hinatsu
***Page 2104***

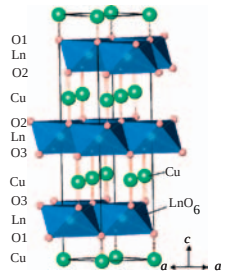


Ternary rare earth oxides $ALnO_2$ ($A$ = Cu or Ag; $Ln$ = rare earths) crystallized in the delafossite-type structure with the rhombohedral 3R poly-type (space group: $R$-3$m$). Magnetic susceptibility measurements showed that these compounds are paramagnetic down to 1.8 K. Specific heat measurements down to 0.4 K indicated that $CuNdO_2$ ordered antiferromagnetically at 0.8 K.

---

**$\{XW_{12}O_{40}[Cu(en)_2(H_2O)]_3\}$ ($X$ = V, Si): Two novel tri-supported Keggin POMs with transition metal complexes**
Yu-Kun Lu, Xiao-Bing Cui, Yan Chen, Jia-Ning Xu, Qing-Bin Zhang, Ya-Bing Liu, Ji-Qing Xu and Tie-Gang Wang
***Page 2111***

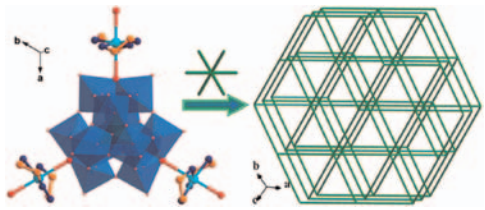

The first classical Keggin polyoxoanion tri-supported by TMC moieties via bridge oxygen atoms, $\{X^{IV}W^{VI}_{10}W^{V}_{2}O_{40}[Cu(en)_2(H_2O)]_3\}$, act as the neutral molecular unit to construct the interesting 3-D supramolecular frameworks.

---

**Structural analysis of the microporous semiconductor K-SBC-1 during its reversible sorption of water**
Alexander Shulman, Vratislav Langer and Anders E.C. Palmqvist
***Page 2118***

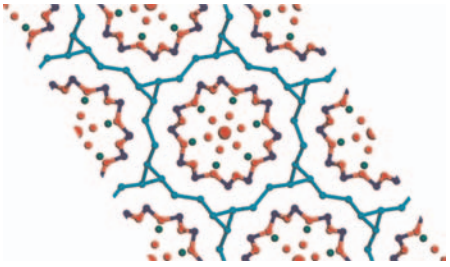

Three crystallographic adsorption sites for water are found in the crystalline microporous semiconductor K-SBC-1. Upon heating to 240 °C the material desorbs enough strongly bound water to become activated for reversible sorption at room temperature, due to redistribution of water occupancy between the strong and weak adsorption sites.

---

**Mesoporous aluminum phosphite**
Jamal El Haskouri, Mónica Pérez-Cabero, Carmen Guillem, Julio Latorre, Aurelio Beltrán, Daniel Beltrán and Pedro Amorós
***Page 2122***

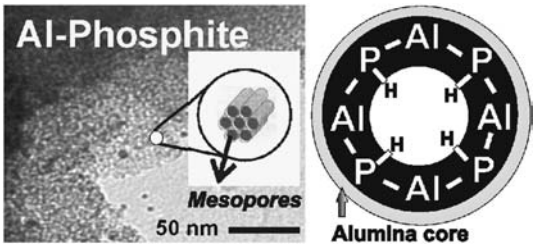


TEM image of the mesoporous aluminum phosphite showing the hexagonal disordered pore array that is generated by using surfactant micelles as template. Also a scheme emphasizing the presence of an alumina-rich core and an ALPO-like pore surface is presented.

---

**Helical polyurethane@attapulgite nanocomposite: Preparation, characterization and study of optical activity**
Zhiqiang Wang, Yuming Zhou, Yanqing Sun, Kai Fan, Xingxing Guo and Xiaolei Jiang
***Page 2130***

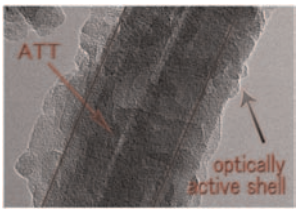


Helical polyurethane@attapulgite (BM-ATT) based on R-1,1′-binaphthyl′,2-diol (R-BINOL) nanocomposite was prepared after surface modification of attapulgite (ATT). This rod-like composite is coated by the optically active polyurethane shell on the surfaces.

---

**Synthesis of magnetic nickel spinel ferrite nanospheres by a reverse emulsion-assisted hydrothermal process**
Jilin Zhang, Jianxin Shi and Menglian Gong
***Page 2135***

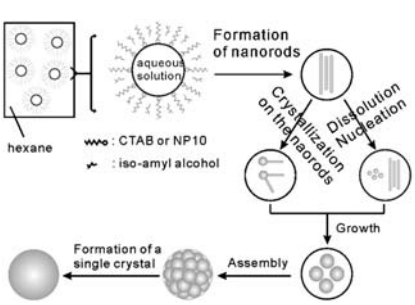


Nickel ferrite nanospheres were obtained through a reverse emulsion-assisted hydrothermal process. The phase transformation as a function of reaction time was studied based on the XRD, TEM and EDS analyses.

**Hierarchical control of porous silica by pH adjustment: Alkyl polyamines as surfactants for bimodal silica synthesis and its carbon replica**
G. Abellán, A.I. Carrillo, N. Linares, E. Serrano and J. García-Martínez
***Page 2141***

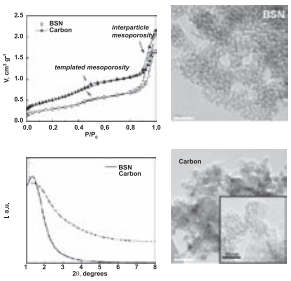


Hierarchical bimodal porous silica and its carbon replica prepared by nanocasting.

---

**Mechanosynthesis of nanopowders of the proton-conducting electrolyte material Ba(Zr, Y)$O_{3-\delta}$**
I. Antunes, A. Brandão, F.M. Figueiredo, J.R. Frade, J. Gracio and D.P. Fagg
***Page 2149***

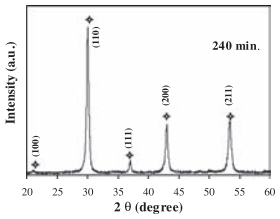


The formation of perovskite nanopowders of the common proton-conducting, electrolyte, material $Ba(Zr_{1-x}Y_x)O_{3-\delta}$ is demonstrated by room temperature mechanosynthesis, starting from $BaO_2$ with $ZrO_2$, $(ZrO_2)_{0.97}(Y_2O_3)_{0.03}$ or $(ZrO_2)_{0.92}(Y_2O_3)_{0.08}$ precursors.

---

**Manganite charge and orbitally ordered and disordered states probed by Fe substitution into Mn site in $LnBaMn_{1.96}Fe_{0.04}O_5$, $LnBaMn_{1.96}Fe_{0.04}O_6$ and $LnBaMn_{1.96}Fe_{0.04}O_{5.5}$ (Ln = Y, Gd, Sm, Nd, Pr, La)**
Alexandre I. Rykov, Yutaka Ueda and Kiyoshi Nomura
***Page 2157***

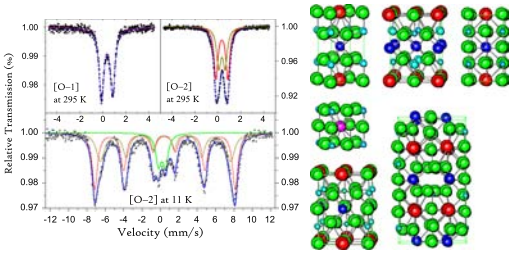


Moessbauer spectra were studied in manganites whose structures were refined with symmetry groups: *P*4/mmm, *P*4/nmm, Pm3*m*, Icma and *P*2.

**Synthesis, network structure and morphology of s-triazine-organosilane glassy hybrid materials**
Isam Arafa, Mazin Shatnawi and Heyam Sàad
***Page 2167***

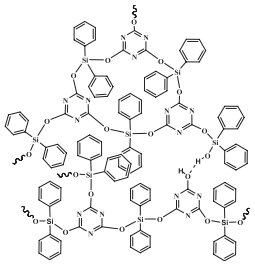

Network structure of s-triazine-organosilane glassy hybrid materials.

---

**A TEM investigation of the $(Bi_{1-x}Sr_x)Fe^{3+}O_{3-x/2}$, $0.2 \le x \le 0.67$, solid solution and a suggested superspace structural description thereof**
R.L. Withers, L. Bourgeois, K. Balamurugan, N. Harish Kumar, P.N. Santhosh and P.M. Woodward
***Page 2176***

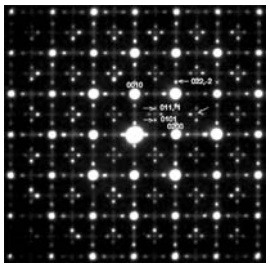

Typical $\langle 100 \rangle_p$ zone axis EDP typical of the $(Bi_{1-x}Sr_x)Fe_1^{3+}O_{3-x/2}\square_{x/2}$, $x \sim 0.55$, sample.

---

**Mesoporous mesocrystal $Ce_{1-x}Zr_xO_2$ with enhanced catalytic property for CO conversion**
Xiazhang Li, Chaoying Ni, Feng Chen, Xiaowang Lu and Zhigang Chen
***Page 2185***

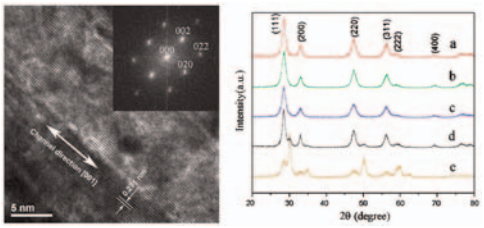


Structure of mesoporous mesocrystal $CeO_2$ with the crystal axis [001] parallel to the pore channel and its phase evolution with various molar fraction of Zr dopant (a) $x = 0$, (b) $x = 0.2$, (c) $x = 0.3$, (d) $x = 0.5$, and (e) $x = 0.8$.

*Continued*

**Mild hydrothermal synthesis, crystal structure, spectroscopic and magnetic properties of the $[M^{II}_{x}M^{III}_{2.5-x}(H_2O)_2(HP^{III}O_3)_y(P^{V}O_4)_{2-y}F]$ [$M$ = Fe, $x$ = 2.08, $y$ = 1.58; $M$ = Co, Ni, $x$ = 2.5, $y$ = 2] compounds**
Joseba Orive, José L. Mesa, Estibaliz Legarra, Fernando Plazaola, María I. Arriortua and Teófilo Rojo
***Page 2191***

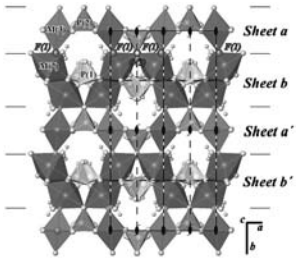


Polyhedral view of the crystal structure of the $[M^{II}_{x}M^{III}_{2.5-x}(H_2O)_2(HP^{III}O_3)_y(P^{IV}O_4)_{2-y}F]$ [$M$ = Fe, $x$ = 2.08, $y$ = 1.58; $M$ = Co, Ni, $x$ = 2.5, $y$ = 2] compounds showing the sheets along the [001] direction.

**Hydrothermal synthesis and characterization of two new layered vanadium tellurites $Cu(TATP)V_2TeO_8$ and $Cu(DPPZ)V_2Te_2O_{10}$**
Guang-Xi Han, Yong-Juan Song and Zheng-Bo Han
***Page 2202***

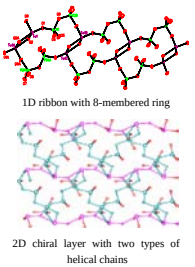


The changes of the size of the rigid aromatic chelate ligands may influence the structures of the V–Te–O framework.

**Hydrothermal syntheses, structures, and magnetic properties of $(NH_4)_2NaVF_6$ and $Na_3VF_6$**
Lijie He, Hongming Yuan, Keke Huang, Chen Yan, Guanghua Li, Qiaoru He, Yang Yu and Shouhua Feng
***Page 2208***

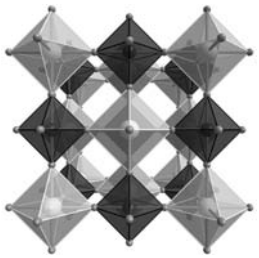

The single crystals of perovskite fluorides $(NH_4)_2NaVF_6$ and $Na_3VF_6$ were synthesized under mild hydrothermal conditions. $(NH_4)_2NaVF_6$ has a cubic elpasolite-type structure and crystallizes in the space group $Fm\bar{3}m$ with lattice constant $a$ = 8.495(0) Å. The compound of $Na_3VF_6$ has a monoclinic structure and in space group $P2_1/n$. The hydrothermal synthesis, structural characterization and magnetic properties of the two compounds were investigated.

**Water molecule-enhanced $CO_2$ insertion in lanthanide coordination polymers**
Liushan Luo, Xiaoyuan Huang, Ning Wang, Hongyan Wu, Wenbin Chen, Zihao Feng, Huiping Zhu, Xiaoling Peng, Yongxian Li, Ling Huang, Shantang Yue and Yingliang Liu
***Page 2213***

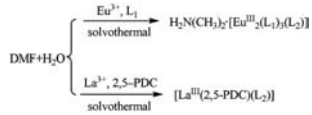


Two new lanthanide coordination polymers involving water molecule-enhanced $CO_2$ insertion resulting in the formation of formic anion and dimethylammonium cation were synthesized under solvothermal conditions.

**Visible quantum cutting through downconversion in $GdPO_4:Tb^{3+}$ and $Sr_3Gd(PO_4)_3:Tb^{3+}$**
Deyin Wang and Nobuhiro Kodama
***Page 2219***

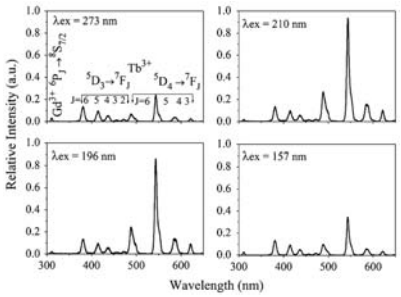


The ratio of emission from $^5D_4$ level to that attributed to $^5D_3$ of $Tb^{3+}$ and $^6P_J$ of $Gd^{3+}$ under 210,196 and 157 nm excitations are much stronger than that under 273 nm excitation, indicating visible quantum cutting has occurred in $GdPO_4:Tb^{3+}$ upon $Tb^{3+}$ $4f^8$–$4f^7 5d^1$ excitation and host excitation.

**The evolvement of pits and dislocations on $TiO_2$-B nanowires via oriented attachment growth**
Bin Zhao, Feng Chen, Wenwu Qu and Jinlong Zhang
***Page 2225***

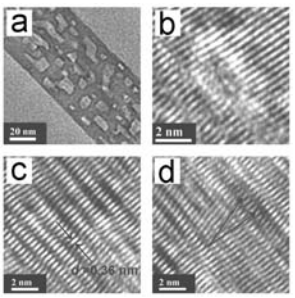


The unique morphology of pits and dislocations on $TiO_2$-B nanowires shown in high-resolution transmission electron microscopy (HRTEM) and a proposed evolvement mechanism of pits and dislocations on $TiO_2$-B nanowires.

**Original close-packed structure and magnetic properties of the $Pb_4Mn_9O_{20}$ manganite**

Artem M. Abakumov, Joke Hadermann, Alexander A. Tsirlin, Haiyan Tan, Jo Verbeeck, Haitao Zhang, Evgeny V. Dikarev, Roman V. Shpanchenko and Evgeny V. Antipov

***Page 2231***

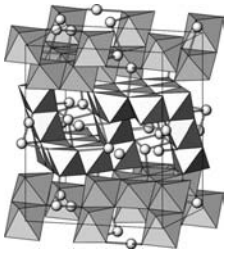

The crystal structure of $Pb_4Mn_9O_{20}$ is based on a 6H $(cch)_2$ close packing of "*h*"-type ($O_{16}$) layers alternating with "*c*"-type ($Pb_4O_{12}$) layers. The Mn atoms occupy octahedral interstices. The $MnO_6$ octahedra share edges within the layers and corners across the layers. Magnetization measurements reveal a tendency towards spin freezing.

---

**Europium substitution into intermetallic phases grown in Ca/Zn flux**

Milorad Stojanovic and Susan E. Latturner

***Page 2239***

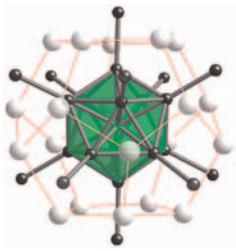

Exploration of europium substitution into intermetallic compounds grown in Ca/Zn flux has yielded analogs of $Eu_xCa_{21-x}Ni_2Zn_{36}$ with unusual magnetic properties due to segregation of europium in the crystals; high concentrations of Eu in the flux trigger the growth of $Eu_{1.63(1)}Ca_{1.37(1)}Ni_2Zn_3$ with a new structure type.

---

**Thermal transformation of quaternary compounds in $NaF–CaF_2–AlF_3$ system**

Julia N. Zaitseva, Igor S. Yakimov and Sergei D. Kirik

***Page 2246***

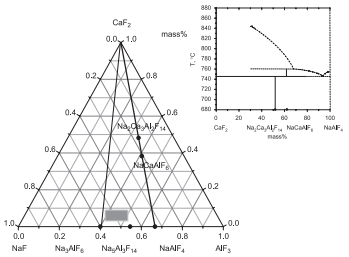


The paper concerns of a small piece of the ternary system ($NaF–CaF_2–AlF_3$) which is very important for aluminum production. Details of phase relations were not fully understand up till now because of experimental difficulties: aggressive reagents and high temperature. However, the phase diagram is very important for production control.

**First discovery and structural characterization of a new compound in Al–Si–O–C system**

Tomoyuki Iwata, Motoaki Kaga, Hiromi Nakano and Koichiro Fukuda

***Page 2252***

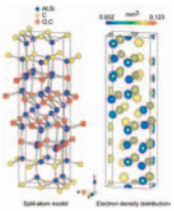

A quaternary oxycarbide firstly discovered in the Al–Si–O–C system. The crystal is an inversion twin, and hence the structure is represented by a split-atom model. The three-dimensional electron density distribution is determined by the maximum-entropy methods-based pattern fitting, being consistent with the disordered structural model.

---

**Synthesis and characterization of $La_{0.8}Sr_{1.2}Co_{0.5}M_{0.5}O_{4-\delta}$ ($M$ = Fe, Mn)**

H. El Shinawi, J.F. Marco, F.J. Berry and C. Greaves

***Page 2261***

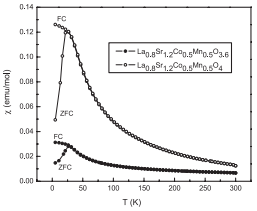


$La_{0.8}Sr_{1.2}Co_{0.5}Fe_{0.5}O_4$ and $La_{0.8}Sr_{1.2}Co_{0.5}Mn_{0.5}O_4$ have been synthesized by a sol–gel procedure and characterized by diffraction techniques, thermal analysis and Mössbauer spectroscopy. Oxide ion vacancies, created via reduction, are located in the equatorial planes of the $K_2NiF_4$-type structure. $La_{0.8}Sr_{1.2}Co_{0.5}Fe_{0.5}O_{3.65}$ shows antiferromagnetic, noncollinear magnetic order, whereas competing ferromagnetic and antiferromagnetic interactions in $La_{0.8}Sr_{1.2}Co_{0.5}Fe_{0.5}O_4$, $La_{0.8}Sr_{1.2}Co_{0.5}Mn_{0.5}O_4$ and $La_{0.8}Sr_{1.2}Co_{0.5}Mn_{0.5}O_{3.6}$ induce spin glass behaviour.

---

**Self-powdering and nonlinear optical domain structures in ferroelastic $\beta'$-$Gd_2(MoO_4)_3$ crystals formed in glass**

Y. Tsukada, T. Honma and T. Komatsu

***Page 2269***

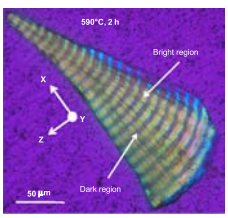


This figure shows the polarized optical photograph at room temperature for a particle (piece) obtained by a heat treatment of the glass at 590 °C for 2 h in an electric furnace in air. This particle was obtained through the self-powdering behavior in the crystallization of glass. The periodic domain structure is observed. Ferroelastic $\beta'$-$Gd_2(MoO_4)_3$ crystals are formed in the particle, and second harmonic generations are detected, depending on the domain structure.

*Continued*

**Visible-light photocatalytic activity of the metastable $Bi_{20}TiO_{32}$ synthesized by a high-temperature quenching method**
Hefeng Cheng, Baibiao Huang, Ying Dai, Xiaoyan Qin, Xiaoyang Zhang, Zeyan Wang and Minhua Jiang
***Page 2274***

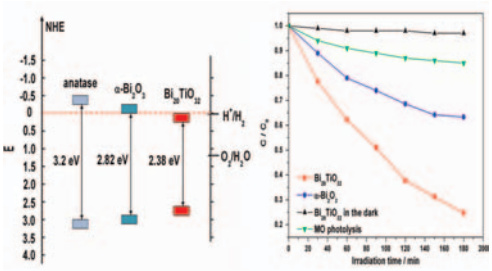


Metastable $Bi_{20}TiO_{32}$ samples were successfully synthesized by a quenching process. Photodegradation against methyl orange showed high visible-light activity and it was supposed to be associated with its corresponding band structure.

**Decorating multi-walled carbon nanotubes with nickel nanoparticles for selective hydrogenation of citral**
Yuechao Tang, Dong Yang, Feng Qin, Jianhua Hu, Changchun Wang and Hualong Xu
***Page 2279***

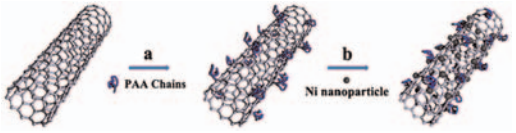


Nickel nanoparticles decorated multi-walled carbon nanotubes (Ni-MWNTs) nanocomposites were conveniently prepared by a chemical reduction of nickel salt in the present of poly(acrylic acid) grafted MWNTs (PAA-*g*-MWNTs). These nanocomposites possessed excellent catalytic activity and selectivity for hydrogenation of citral.

**Field emission of vertically aligned $V_2O_5$ nanowires on an ITO surface prepared with gaseous transport**
Ming-Cheng Wu and Chi-Shen Lee
***Page 2285***

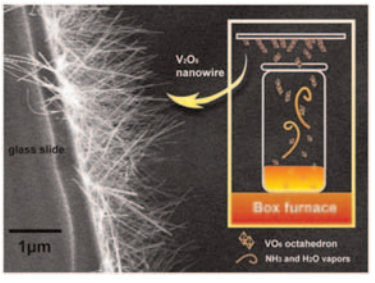


Growing $V_2O_5$ nanowires on a conducting glass substrate combines gaseous transport and pyrolytic deposition of vanadium polyoxometalate anions, and yields vertically aligned vanadium-oxide nanowires.

**Lanthanide-organic frameworks constructed from multi-functional ligands: Syntheses, structures, near-infrared and visible photoluminescence properties**
Xinfa Li, Zailai Xie, Jingxiang Lin and Rong Cao
***Page 2290***

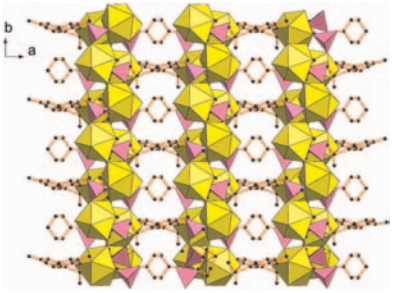


Five multi-functional ligands supported 3D lanthanide-organic frameworks have been synthesized and structurally characterized. Compounds 5 and 3 displayed strong solid-state emissions in the visible and near-infrared region at room temperature.

**Novel symmetrical coralloid Cu 3D superstructures: Solid-state synthesis from a Cu-carboxylate MOF and their in-situ thermal conversion**
Lingyun Chen, Yongming Shen, Junfeng Bai and Chunzhao Wang
***Page 2298***

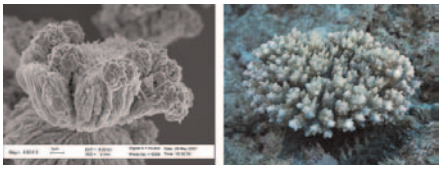

Novel symmetrical coralloid Cu 3D superstructures were synthesized by thermolysis of the $[Cu_3(btc)_2]$ (*btc* = benzene-1,3,5-tricarboxylato) MOF microcrystals in a one-end closed horizontal tube furnace (OCTF).

**A cluster with a mixed $M_6X_{12}/M_6X_8$ environment: The $La_6Cl_{11}Co$ structure**
Chong Zheng, Hansjürgen Mattausch, Constantin Hoch and Arndt Simon
***Page 2307***

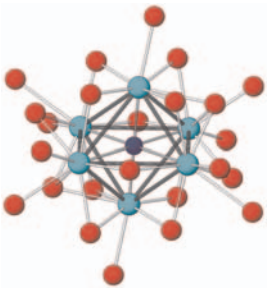

$La_6Cl_{11}Co$ octahedron exhibiting a mixed $M_6X_{12}/M_6X_{12}$ coordination environment.

**Order–disorder phase transformations in quaternary pyrochlore oxide system: Investigated by X-ray diffraction, transmission electron microscopy and Raman spectroscopic techniques**

A.N. Radhakrishnan, P. Prabhakar Rao, K.S. Sibi, M. Deepa and Peter Koshy

***Page 2312***

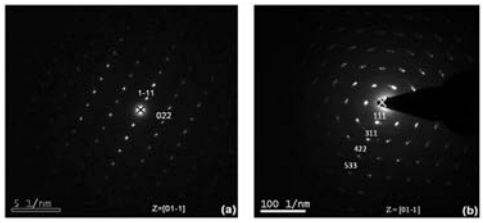


Selected area electron diffraction (SAED) patterns showed highly ordered diffraction maxima with characteristic superlattice weak diffraction spots of the pyrochlore structure for (a) $Ca_{0.6}7Y_{1.33}Zr_{1.33}Ta_{0.33}O_7$ (C2YZT2) and bright diffraction maxima arranged in a ring pattern of the fluorite structure for (b) $Ca_{0.29}7Y_{1.71}Zr_{1.71}Ta_{0.29}O_7$ (CY6Z6T).

**New insight in the structure–luminescence relationships of $Ca_9Eu(PO_4)_7$**

Rajia Ait Benhamou, Aurélie Bessière, Gilles Wallez, Bruno Viana, Mohamed Elaatmani, Mohamed Daoud and Abdelwahed Zegzouti

***Page 2319***

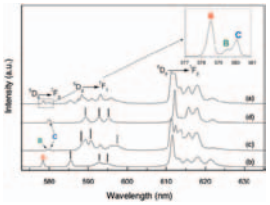


Emission spectra of $Ca_9Eu(PO_4)_7$ recorded at 10 K evidencing the three different sites for $Eu^{3+}$ dopant cation.

**Suppression of spin density wave by isoelectronic substitution in $PrFe_{1-x}Ru_xAsO$**

Michael A. McGuire, David J. Singh, Athena S. Sefat, Brian C. Sales and David Mandrus

***Page 2326***

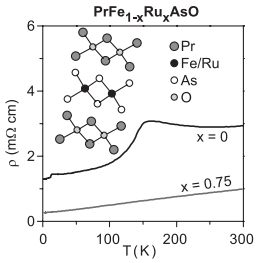


Substitution of Ru for Fe in PrFeAsO completely suppresses the spin density wave transition without the occurrence of superconductivity at temperatures above 2 K.

## *Corrigendum*

**Corrigendum to "Preparation and luminescence properties of $Ce^{3+}$ and/or $Tb^{3+}$ doped $LaPO_4$ nanofibers and microbelts by electrospinning" [Journal of Solid State Chemistry 182 (2009) 698–708]**

Zhiyao Hou, Milin Zhang, Lili Wang, Hongzhou Lian, Ruitao Chai, Cuimiao Zhang, Ziyong Cheng and Jun Lin

***Page 2332***